STUDENT PAPER

AIRBORNE UAV REMOTE SENSOR POSITION ACCURACY ALGORITHM IN CATASTROPHES ZONES

Vipinkumar Rajendra Pawar
Ph. D. Scholar
Terna Engineering College
Mumbai University
Mumbai-400 706, India
Email : vipinkumar.research@gmail.com
research@vipinpawar.in

Sudhakar S. Mande
Professor
Don Bosco Institute of Technology
Mumbai-400 706, India

Imdad Rizvi
Professor
Terna Engineering College
Mumbai University
Mumbai-400 706, India
and
Visiting Professor
Higher College of Technology
Sharjah Campus, UAE

Abstract

Sensor payload calibration and FOV are still the most essential parameters in Airborne Remote Sensors for developing quality terrain images in the Remote Sensing field. UAVs are core devices in Airborne Remote Sensing by carrying camera payload for large terrain objects to achieve desired image quality with geographical position provided for different available flight planning algorithms.

This paper proposes the algorithm to find the exact Geo-coordinates for UAV navigation algorithm viewpoint identification for implementing Airborne Remote Sensing (ARS) to study Landslide Susceptibility Zone as well as application for catastrophe analysis. Terrain Slope and Aspect was considered using Remote Sensing products from ISRO CartoSat and NASA ASTER satellite available in the Digital Elevation Model (DEM) construction to maintain the calibrated angle of vision, field of vision, and land surface image quality.

This algorithm will enhance the functioning of various available UAV Flight Planning Algorithms to improve the quality of 3D topography images for 3D Modeling as well as Landslide and Flood Prediction and Analysis, as well as provide the position of camera payload and tilting angle for enhanced terrain images.

Keywords*: ARS, ISRO, DEM, LISS III, LSI, SI, LRI, OSM, NDVI,VI*

Abbreviations

ARS = Airborne Remote Sensing
ISRO = Indian Space Research Organisation
DEM = Digital Elevation Model
LISS III = Linear Imaging Self Scanner 3
LIS = Landslide Susceptibility Zone

Paper Code : V72 N4/1089-2020. Manuscript received on 26 Apr 2020. Reviewed, Revised and Accepted as a Student Paper on 09 Nov 2020

SI = Slope Index
LRI = Landslide Risk Index
OSM = Open Street Map
NDVI = Normalized Differential Vegetation Index
VI = Vegetation Index

Introduction

Airborne Remote Sensing (ARS) in Disaster Assessment

Airborne Remote Sensing (ARS) is a most popular technique for collecting information from multi-directional angle of view about specific terrain profile. An analysis of any terrain profile becomes easier [1] due to multi-directional graphical visualization. Aerial photography is usually the most popular concept for ARS gathering data. Planes, gliders, drones, and quad-copters are generally used for aerial photography to collect photographs of specific terrain. Now, a few days by using UAV technology, ARS applications grew rapidly [2].

UAV Role in ARS for Disaster Assessment

Natural disasters are non-ignoring tragedies which cannot be controlled and predicted by human actions. But we can predict the pre-activities of natural disasters to a certain extent by monitoring the pre-released symptoms to reduce the loss to humans. In this paper we focused as an area of study on Landslide Susceptibility Zones. Analysis of natural disaster hazard and victim analysis, to take real-time photographs of disaster-prone areas, it is necessary to deploy algorithmic UAVs.

Because of large geological bodies such as rock, terrain slopes, traditional survey methods are time-consuming and the results are univariable, which can misjudge geological surface constancy. The most common techniques used in the field of natural slopes are Digital Photography (DP). An IoT model of Unmanned Aerial Vehicles (UAVs) connected via wireless intercommunicate can identify and verify the strength of a disaster [4, 5, 6].

UAV applications in cataclysm governance deviate according to responsibility during different stages of catastrophe governance and classified broadly as shown in Fig.1. Also, implementation of discharge navigation panel by factor-based UAVs for catastrophe hazard diminution is practical possibilities. Generally speaking, software agents generate UAV discharge guidance plans and pick out the safest navigation as a discharge support path taking into account disaster situations and territorial characteristics, etc. Additionally, UAVs provide efficient guidance for discharge by group action of other UAVs [6].

Considering the role of UAVs for assessing risk and analyzing Landslide Susceptibility Zone in Natural Disaster, the performance of UAV flight planning needs to be optimized by providing precise geo-location in the form of WGS84 coordinate systems such as Longitude, Latitude and Altitude of Snapping Point as shown in Fig.2.

In this paper, the exact problem statement identified by taking into account the reduced quality of the images obtained by UAVs only because of unguided field of view. Exact methodology was proposed using remote sensing data collected from Satellite image (ISRO-Cartosat and NASA: USGS-Aster DEM) to identify the exact UAV position co-ordinates for perfect camera field view adjustment. To predict the Landslide Susceptibility Zone stated the Digital Elevation model is used to identify the terrain slopes. The Landslide Prone area that is generally mapped in the red zone shown if Fig.18 has a high risk of landslide. This mapped area is the exact location where UAV images should be taken.

The direction of the slope is calculated in in the form of aspect, which is the most effective parameter while identifying UAV position. The combined section provides the exact area of susceptibility to landslides where pre-disaster monitoring is required using UAV. This area is now classified as a UAV camera field of view. Results shows the center of image comparative table and the field of view perpendicular axis so that we can identify UAV's practical location in three dimensional parameters.

Problem Statement

Augmented Reality (AR) technology requires 3D images which need to be developed in ARS to enhance the catastrophe-pronounced region 3D model. The camera's angle of vision must be set in such a way that the image area center must be in a line of sight [7]. The angle of vision is the degree of perception of the observable object at any moment. In the case of optical payload, what a gauge is empathetic to electromagnetic radiation is a solid angle concluded. The exact content [7, 8] may otherwise be stretched to image formation.

UAVs arise as a perfect technology for image acquirement due to advanced mobility in complicated and heavily built environments. The non-heritable images can be used

to generate high-quality 3D models using multidirectional view strategies to photography. However, the reliability of the subsequent 3D framework is heavily dependent on the predictive flight plan, which still requires skilled human expertise, especially in intricate and uneven urban and hazardous environments.

It is crucial when taking an image to affiliate as many coded citation point markers as possible diffuse over the whole object to achieve a high measuring quality as shown in Fig.3 [10]. The actual problem statement is that in processing a deep-performance and authentic 3D multispectral image analysis device, milestones are primarily traced from the proceeding parameters: appropriate sensor positioning and location and FOV (Field of View) with angle as shown in Fig.4, rich and in exiled systemic design, trustworthy and precise data processing and precise multisensor data combination. The Field of View (FOV) for each spectroscopy unit should always be assigned appropriately to accommodate the estimated area, as shown in Fig.2. In this scenario, during assembly and examination phases, certain methods should be used to configure the mechanical system to make better adjustment of the sensors. Most units of data capture should generally have some angle of inclining or rotational freedom. When assembling a unit, it should be positioned tightly with the location marked for each unit, so that the remount and assembly of the unit can be positioned in exactly the same position [9].

UAVs may be mounted at varying altitudes, based on the environmental conditions and the demands of the customers. However, the coverage area also varies [11] by modifying the altitude of the UAVs.

Under WGS84 (Global Geographical Coordinate System Standard) [16], the 3D placement infused linear scheduling problem of UAVs was investigated in order to get the best placement in inclined direction in the form of latitude and longitude, altitude, and users. Used best trajectory improvement and service location issues as a tool around using multiple UAVs to the improved 3D deployment.

Positioning algorithm is currently being developed by [14], where 2D plane surface is used to estimate the location of UAV for photography. Figs.5 and 6 shows the location the UAV and the point of reference on the 2D plane; reported to standard imaging algorithm, the position of target as shown in Fig.6, object U = [x_0; y_0; z_{min}] can be estimated by[14].

$$X_o = \frac{h}{Z_b} X_b \; ; \; Y_o = \frac{h}{Z_b} Y_b \; ; Z_{\min} = 0 \tag{1}$$

In reference [15], 3D Placement of UAV in 3 axis coordinate system is proposed. As shown in Fig.6, location (x_o; y_o; z_{min}) is expected flight location of UAV unfortunately, while dealing with external environment, UAV must have to navigate through (X,Y, Z) = (Longitude, Latitude, Altitude) navigation coordinates systems. In Ref.[15], the respective algorithm fails to predict the identification of the geocoordinate location.

To find out exact and accurate geographical location and elevation of UAV for Natural Disaster Analysis using Closed Range Photogrammetry, Algorithm stated in this paper is the final and finest solution to find accurate UAV geo-coordinates in 3 axis, mean in the form of (Length, Latitude, Altitude).

In this algorithm we can obtain the exact geo-coordinates of the UAV snapping point in the form of Longitude, Latitude and Elevation as shown in Fig.7.

Methodology

Identification of WSN Cluster for Landslide Prone Area

Landslide Index (LI)

Landslide Index is slope elevation index range from 0 to 1 where 0 means at surface and 1 means extremely heavy gradient. it is formulated as,

$$Slope \;\; Index \; (SI) \; = \; slope / 90 \tag{2}$$

Slope is maximum rate of change in pixel of DEM with respect to its neighbor. Slope is measured in units of degrees as shown in Fig.8.

$$Slope \; = \; \tan \left(\frac{d\,z}{d\,x} \right)^2 * \left(\frac{d\,z}{d\,y} \right)^2 * \frac{180}{\pi} \tag{3}$$

Colored raster image obtained after slope equation mentioned in Eq.(3) will be shown in Fig.9 while using above formula, we have to take care the following things, consider 3 x 3 matrix is used as shown in Fig.10 to calculate slope from ‘e’,

$$\frac{d\,Z_{\min}}{dx} \; = \; \frac{((\,c + i + 2f\,)\,(a + g + 2d\,))}{8\;Y_{cell\;size}} \tag{4}$$

The rate of change in the x direction for cell 'e' is calculated as,

$$\frac{d Z_{\min}}{dy} = \frac{((g + i + 2h)(a + c + 2b))}{8 X_{cell\ size}} \quad (5)$$

Landslide Slope Index (LSI)

Landslide Index is slope elevation index range from 0 to 1 where 0 means at surface and 1 means extremely heavy gradient. it is formulated as,

$$Landslide\ \ Slope\ \ Index\ (LSI) = \frac{Slope}{90} > 30^{o} \quad (6)$$

Slope is maximum rate of change in pixel of DEM with respect to its neighbor.

$$0 < LSI < 0.3 \quad (7)$$

Landslide Slope Index (LSI) shown in Fig.13, the maximum slope indicated in red, yellow and green for colour reference. Where red indicates heavy slope, yellow indicates moderate slope, and green indicates very low prole slope. LSI ranges from 0.3 to 1, because landslide will normally be responsible for 30 degrees or more of the slop profile.

Landslide Prone Area

Landslide prone area is defined as the exact populated area where both living things and infrastructure can be damaged by landslide. It means that landslide normally occurred anywhere with low vegetation where heavy terrain profile is available. But all the landslides did not affect human life. Only those landslides affect the living thing that occurs either in the area of the city or on the road. So identify such areas as Landslide Prone Area (LPA). OpenStreet Map (OSM) provides accurate analysis of road and city area with road vector data, highways in form line and city area in polygon form. Such an area has been identified as a Landslide Risk Index (LRI) intersection and a vectored road and urban zone area.

$$LPA = LRI \cap Road \cap LRI\ \ Urban \quad (8)$$

Intersection of the landslide risk index and the road and urban area to determine the exact susceptible landslide zone where the actual sensor network needs to be deployed.

Landslide Wireless Sensor Network Cluster Zone (LCZ)

Normally landslides occurred at any area of heavy terrain profile, but not all are responsible for loss of life or human. Landslide Prone is the intersection of Landslide sensitive area with continuous human movement civilization, normally road and urban areas. The landslide area closer to the road and urban area must therefore be considered as the Landslide Prone area which may be responsible for serious loss of life.

$$LCZ = LRI + LPA \quad (9)$$

From equation LRI and LSI, LCZ can be calculated as below,

$$LCZ = LRI + \left[\frac{LRI}{Road_{vectored}} + \frac{LRI}{City_{vectored}}\right] \quad (10)$$

DEM Slope Direction

While dealing with terrain slope, slope direction also makes more impact in disaster-prone area prediction as flood direction and debris flow direction is related to any mountain's slope direction. Slope direction term is used from 0 degree to 360 degree.

As shown in g.11, 0 degree means north direction, 90 degree represents east direction, 180 degree refers to south direction and 270 degree refers to west diet as shown in Fig.11 respectively. And related aspect image shown in Fig.12. Considering the change per unit for cell 'e' in both the x_o and y_o direction, slope direction is calculated using:

$$Slope\ \ Direction = 57.29 * atan\ 2\left(\frac{d z_{\min}}{d y}, \frac{d z}{d x}\right) \quad (11)$$

Identify Risk Zones

The center of vision angle for UAV imagery is Centroid of all landslide risk zones. But the Optimized Geopositioning algorithm for UAV needs to be used as derived and justified in this paper to identify the exact geographical location and height of UAV for taking proper image with perpendicular surface. Fig.13 shows that image size Bi x Bi has been taken. And camera payload with focal angle installed on the drone. It is considered that, as shown in Fig.14, the image taken from the surface is completely at with no slope.

Consider point A as a drone camera payload having a focal angle of according to the following geometry. Image must be taken with W width i.e. Length BC. Image center is point D which is image center as shown in Fig.15.

Terrain Slope means: Slope direction of the terrain is given by. In the cartesian coordinate system, when dealing with geocoordinate latitude and longitude, it is considered as x-y co-ordinates to find the exact location of the drone in the geographic area as shown in Figs.15 and 16.

The Z value always indicated object height with surface reference. Z values are always measured in meters. And in WGS84 system Geocoordinates are recorded. While determining the specific distance with a specific direction using Latitude and Longitude, the geo-coordinate constant should be considered.

$$f(x) = \frac{W}{2}\left[\frac{\cos\theta}{\sin\theta} * \cos\alpha\right] * 0.00000625 \quad (12)$$

Where, 1 meter = 0.00000625 map units. It has been deriving the latitude by considering slope and aspect, and $\theta = 90 - \alpha$

$$Latitude_{Drone\ Position} = [f(x) * \cos\beta] + Latitude_{centroid} \quad (13)$$

Also can be deriving longitude of drone position as,

$$Longitude_{Drone\ Position} = [f(x) * \cos\beta] + Longitude_{centroid} \quad (14)$$

To find the expected height of UAV payload with reference to surface, We can state that with the reference to above image,

$$Distance\ AE = \frac{W}{2}\left[\frac{\cos\theta * \cos\alpha}{\sin\theta}\right] * \frac{\sin\alpha}{\cos\alpha} \quad (15)$$

Modification of above equation will cancel cos α

$$Distance\ AE = \frac{W}{2}\left[\frac{\cos\theta * \sin\alpha}{\sin\theta}\right] \quad (16)$$

So final equation of drone height will be,

$$Distance\ AE = \frac{W}{2}\left[\frac{\sin\alpha}{\tan\theta}\right] \quad (17)$$

But distance AE is height difference between Centroid of Image and expected UAV height, in order to find the exact elevation above the surface, it is necessary to add centroid elevation of the image taken from DEM imagery. So, exact height of UAV from above surface is noted as Z0,

$$Distance\ AE = \frac{W}{2}\left[\frac{\sin\alpha}{\tan\theta}\right] + Z_i \quad (18)$$

Where Z_i is the height of centroid of image from surface collected from DEM imagery.

Results

Landslide prediction analysis has different parameters, such as rainfall, slope, density of vegetation and catchment of water, and much more. But fundamental parameters are the slope index, in which the slope of the surface makes more impact on the analysis of landslide predictions. Thus, the slope index has been considered for Landslide Susceptibility area identification by considering the importance and fundamental aspect of landslide. The use of slope index above 0.3 results as shown in Fig.17.

Area of interest is taken from the hill station of Saputara, Gujrat, located near the border of Maharashtra-Gujrat territory in India as shown in Fig.18. Heavily sloped hills and mountains surround this area. And there are lots of terrain variations, too. This area comes under a zone of heavy rainfall. The Landslide Slope Index identifies such zones of susceptibility to landslides.

For UAV image acquisition all Landslide susceptibility zones are considered as a single image of interest. Thus, the center of the individual landslide sensitivity zone is regarded as the center of the image as shown in Fig.18.

Individual flag represents the center of the single image. By applying UAV's Optimized Geo-positioning algorithm, we will obtain exact X-Y coordinates of Drone positioning in the WGS84 coordinate system as shown in Fig.19.

To find the expected altitude for UAV for individual flag point,

$$Z_0 = \frac{W}{2}\left[\frac{\sin\alpha}{\tan\theta}\right] + Z_i \quad (19)$$

Where, Z_i represents elevation of individual ag point units in meters taken from DEM imagery and $\alpha = 90 - \delta$ (*slope*) in degree.

Figure 20 represents Landslide Susceptibility Index (LSI) flag point and Optimized Geo-positioning algorithm for UAV-based actual positioning. Magnification of the individual LSI zone is indicated as here, the flag point representing the centroid of the Landslide Susceptibility Zone and Flight Point representing the actual optimized viewpoint position or also referred to as camera position. In this case, the flag point is located at location 72.739914:20.646661 at a surface elevation of 481 meters. But considering the slope index as, 33.00309 degree with aspect 36.369198 degree, perpendicular line of sight for focal length of camera payload gives the optimized location 11.61057522 meters away from flag point with elevation at 488.262846 meters from surface.

In another case as shown in Figs.20, 21 and 22, the flag point is located at location 72.740731:20.645318 at an elevation of 512 meters from the surface with reference to Table-1 test area. But considering the slope index as, 33.073549 degree with aspect 33.578812 degree, perpendicular line of view for Focal length of camera payload gives the optimized location 11.90099797 meters from flag point with elevation at 519.494435 meters from the surface as shown in Table-2 in result data.

Table-1 : Test Area

Id	Longitude (Flag Point)	Latitude (Flag Point)	Elevation (in Meter)
1	73.55777778	20.7950203	228
2	73.80916667	20.7950203	446
3	73.81847222	20.7950097	470
4	73.87154231	20.79473843	535
5	73.93138889	20.79492367	941
6	73.95844944	20.79494142	828
7	73.96166667	20.79486111	812
8	73.81751621	20.7945688	495
9	73.90860541	20.79445014	546
10	73.96304986	20.79445014	810
11	73.81722222	20.79416667	499
12	73.8729312	20.79418287	538
13	73.9260509	20.7944582	752
14	73.94890208	20.79440642	861
15	73.55804986	20.79389459	219

Table-2 : Result Data

Optimized Latitude	Optimized Longitude	Zi (in Meter)	Z dist (Height from Flag Point)	Distance of UAV from Flag Point in Meter
20.795018	73.557775	235.3376	7.33761175	7.361405371
20.795045	73.809191	453.4073	7.407331947	14.07267037
20.794999	73.818462	477.3545	7.244548744	7.701821813
20.794766	73.871569	542.4919	7.491853811	292.9426126
20.794905	73.93137	948.4163	7.416343889	9.317594166
20.794908	73.958416	834.5514	6.551378754	22.6180366
20.794832	73.961638	819.3316	7.331645475	202.2138202
20.794558	73.817505	502.344	7.344026554	7.839422524
20.794462	73.908618	553.4967	7.49665997	8.127066701
20.794436	73.963036	817.4964	7.496373209	8.368531718
20.794148	73.817204	506.3951	7.395071552	9.203773273
20.794207	73.872955	545.4541	7.454084178	13.62141203
20.794482	73.926074	759.1993	7.19929751	11.04652303
20.794374	73.948869	867.8514	6.851413171	44.54019117
20.793902	73.558058	226.3647	7.364685117	7.580812471

Figure 23 shows an average difference in flag point with respect to optimized UAV location. After analyzing the total of 4340 flag points near Saputara, it is observed that the optimized location is 44 meters from the flag point on average.

Conclusion

Multiple flight planning algorithms are carefully investigated in this work, with their bugs related to image acquisition procedure. Further in this work an algorithm is proposed and successfully implemented to provide precise snapping location to achieve high-quality image without changing the image aspect ratio by identifying exact Goe-Coordinates with parameters of Latitude, Longitude and Altitude of camera snapping point.

Implementation of the proposed algorithm shows that the average distance correction factor of minimum and maximum is 6.1138 m and 292.942613 m respectively, which is away from the flag point. From the results obtained as shown in Fig.21, it is observed that, while developing flight planning algorithms, previous algorithms focus only on the elevation profile but haven't take care of the terrain slopes as per justification in the Table-1 and Table-2.

Proposes Algorithm will improve the path and direction of Phantom's camera angel Version I, II, III, and IV and DJI drones to achieve perfect focused area shots on open environment.

Data Availability Statement

The data that support the findings of this study are openly available within the article and its supplementary material.

Acknowledgement

Author is very greatfull to OpenCellID, NASA Earth Observation (NEO), United States Geological Survey (USGS) Earth Explorer (EE) and ISRO (Bhuvan) for providing technical material for developing the algorithm. Also would like to express sincere gratitude towards Dr. S. S. Mande and Dr. Imdad Rizvi, for the help, leadership and praise provided during entire work. This work would have not been possible without their prized time, patience and motivation. I thank them for making my stint scrupulously pleasant and enriching. I take the privilege to denite my sincere thanks to my family, friends and well-wishers for providing the continuous support.

References

1. Gomez, C. and Purdie, H., "UAV- based Photogrammetry and Geocomputing for Hazards and Disaster Risk Monitoring:, A Review. Geoenvironmental Disasters, 2016, 3 (1).

2. Kenta Katayama., Hideyuki Takahashi., NobuhideYokota ., Kazuya Sugiyasu., Gen Kitagata and Tetsuo Kinoshita., "An Effective Multi-UAVs-based Evacuation Guidance Support for Disaster Risk Reduction", IEEE, 2019, 978-1-5386-7789.

3. Ejaz, W., Azam, M. A., Saadat, S., Iqbal, F. and Hanan, A., "Unmanned Aerial Vehicles Enabled IoT Platform for Disaster Management", Energies, 12 (14), 2019, 2706.
doi:10.3390/en12142706

4. Ejaz, W., Azam, M. A., Saadat, S., Iqbal, F. and Hanan, A., "Unmanned Aerial Vehicles Enabled IoT Platform for Disaster Management", Energies, 12 (14), 2019, 2706.
doi:10.3390/en12142706

5. Meyers, G., Zhu, C., May eld, M., Tingley, D.D., Willmott, J. and Coca, D., "Designing a Vehicle Mounted High Resolution Multi-Spectral 3D Scanner: Concept Design", Proceedings of the 2nd Workshop on Data Acquisition to Analysis, November, 2019, pp.16-21.

6. Chi Liu, I., Xiaoli Liu, I., Xiaochu Peng, I., Enzhi Wang, I. and Sijing Wang., "Application of 3D-DDA Integrated with Unmanned Aerial Vehicle Laser Scanner (UAV-LS) Photogrammetry for Stability Analysis of a Blocky Rock Mass Slope", Landslides, Springer-Verlag GmbH Germany Part of Springer Nature 2019, May 2019.
doi: 10.1007/s10346-019-01196-6

7. El-Din Fawzy, H., "Study the Accuracy of Digital Close Range Photogrammetry Technique Software as a Measuring Tool", Alexandria Engineering Journal, 58(1), 2019, pp.171-179.
doi:10.1016/j.aej.2018.04.004

8. Ur Rahman, S., Kim, G.-H., Cho, Y.-Z. and Khan, A., "Positioning of UAVs for Throughput Maximization in Software-defined Disaster Area UAV Com-

munication Networks", Journal of Communications and Networks, 20 (5), 2018, pp.452-463.

9. Koch, T., Korner, M. and Fraundorfer, F., "Automatic and Semantically-Aware 3D UAV Flight Planning for Image-Based 3D Reconstruction", Remote Sensing, 11 (13), 2019, 1550.
10. Goda, I., Hostis, G.L. and Guerlain, P., "In-situ Non-contact 3D Optical Deformation Measurement of Large Capacity Composite Tank Based on Close-range Photogrammetry", Optics and Lasers in Engineering, 119, pp.37-55.
11. Shakoor, S., Kaleem, Z., Baig, M. I., Chughtai, O., Duong, T. Q. and Nguyen, L. D., "Role of UAVs in Public Safety Communications", Energy Efficiency Perspective. IEEE Access, 2019, p.1.
12. Russo, M., Carnevali, L., Russo, V., Savastano, D. and Taddia,Y., "Modeling and Deterioration Mapping of Facades in Historical Urban Context by Close-range Ultra Lightweight UAVs Photogrammetry", International Journal of Architectural Heritage, 2018, pp.1-20.
doi:10.1080/15583058.2018.1440030
13. Bor-Yaliniz, R. I., El-Keyi, A. and Yanikomeroglu, H., "Efficient 3-D Placement of an Aerial Base Station in Next Generation Cellular Networks", Proceedings of IEEE International Conference Communication (ICC), Kualalumpur, Malaysia, May, 2016, pp.1-5.
14. Lin, L., Yang, Y., Cheng, H. and Chen, X., "Autonomous Vision-Based Aerial Grasping for Rotorcraft Unmanned Aerial Vehicles", Sensors, 19 (15), 2019, 3410.
15. Wang, D., Bai, B., Zhang, G. Han, Z., "Optimal Placement of Low-Altitude Aerial Base Station for Securing Communications", IEEE Wireless Communications Letters, 2019, p.1.
16. Bor-Yaliniz, R. I., El-Keyi, A. and Yanikomeroglu, H., "Efficient 3-D Placement of an Aerial Base Station in Next Generation Cellular Networks", Proceedings of IEEE International Conference Communication (ICC), Kuala Lumpur, Malaysia, May, 2016, pp.1-5.
17. Park, S. and Jung, D., "Vision-Based Tracking of a Ground-Moving Target with UAV", International Journal of Aeronautical and Space Sciences, 2019.
18. "NASA Earth Observation Population Map", 23 April, 2020. https://neo.sci.gsfc.nasa.gov/view.php/datasetId=SEDACPOP
19. "OpenCellID LTE Network Map", 23 April, 2020. https://unwiredlabs.com/coverage
20. Lynn M. Highland (United States Geological Survey) and Peter Borowsky (Geological Survey of Canada)., "The Landslide Handbook| A Guide to Understanding Landslides", U. S. Geological Survey.
21. Shakoor, S., Kaleem, Z., Baig, M. I., Chughtai, O., Duong, T. Q. Nguyen, L. D., "Role of UAVs in Public Safety Communications: Energy Efficiency Perspective", IEEE Access, 2019.
22. Castellanos, G., Deruyck, M., Martens, L. and Joseph, W., "Performance Evaluation of Direct-Link Backhaul for UAV-Aided Emergency Networks", Sensors, 2019.
23. Wang, D., Bai, B., Zhang, G. and Han, Z., "Optimal Placement of Low-Altitude Aerial Base Station for Securing Communications", IEEE Wireless Communications Letters, 2019.
24. Mayor, V., Estepa, R., Estepa, A. Madinabeitia, G., "Deploying a Reliable UAV-Aided Communication Service in Disaster Areas", Wireless Communications and Mobile Computing, 2019.
25. Hu, S., "On Ergodic Capacity and Optimal Number of Tiers in UAV-Assisted Communication Systems", IEEE Transactions on Vehicular Technology, 2019.
26. Ejaz, W., Azam, M. A., Saadat, S., Iqbal, F. and Hanan, A.,"Unmanned Aerial Vehicles Enabled IoT Platform for Disaster Management", Energies, 2019.
27. Koksal, N., Jalalmaab, M. and Fidan, B., "Adaptive Linear Quadratic Attitude Tracking Control of a Quadrotor UAV Based on IMU Sensor Data Fusion", Sensors, 2018.

28. Malandrino, F., Chiasserini, C.-F., Casetti, C., Chiaraviglio, L. Senacheribbe, A., "Planning UAV Activities for Efficient User Coverage in Disaster Areas", Ad Hoc Networks, 2019.

29. Zhao, N., Lu, W., Sheng, M., Chen, Y., Tang, J., Yu, F. R. Wong, K.-K., "UAV-Assisted Emergency Networks in Disasters", IEEE Wireless Communications, 2019.

30. Andrey V. Savkin and Hailong Huang., "Range-Based Reactive Deployment of Autonomous Drones for Optimal Coverage in Disaster Areas", IEEE, 2168-2216, 2019.

31. Tomislav Radisic., Mario Mustra and PetarAndrasi, "Design of an UAV Equipped with SDR Acting as a GSM Base Station", IEEE, 2019.

32. Joe Khalife and Zaher M. Kassas., "Opportunistic UAV Navigation with Carrier Phase Measurements from Asynchronous Cellular Signals", IEEE, 2019.

33. Fan, D., Gao, F., Ai, B., Wang, G., Zhong, Z., Deng, Y. and Nallanathan, A., "Channel Estimation and Self-Positioning for UAV Swarm", IEEE Transactions on Communications, 2019.

34. Perabathini, B., Tummuri, K., Agrawal, A. and Varma, V. S., "Efficient 3D Placement of UAVs with QoS Assurance in Ad Hoc Wireless Networks", 28th International Conference on Computer Communication and Networks (ICCCN)", 2019.

35. Miao, W., Luo, C., Min, G., Wu, L., Zhao, T. and Mi, Y., "Position-Based Beamforming Design for UAV Communications in LTE Networks", IEEE International Conference on Communications (ICC), 2019.

36. William D. Ivancic., Ohio Robert J. Kerczewski., Ohio Robert W. Murawski., Ohio Konstantin Matheou and Ohio Alan N. Downey., "Flying Drones Beyond Visual Line of Sight Using 4G LTE: Issues And Concerns", IEEE, 2019.

37. Park, S. and Jung, D., "Vision-Based Tracking of a Ground-Moving Target with UAV", International Journal of Aeronautical and Space Sciences, 2019.

38. "NASA Earth Observation Population Map" April, 2020. https://neo.sci.gsfc.nasa.gov/view.php?datasetId=SEDACPOP

39. "OpenCellID LTE Network Map" April 2020. https://unwiredlabs.com/coverage

40. Lynn M. and Peter Bobrowsky., "The Landslide Handbook : A Guide to Understanding Landslides", U.S. Geological Survey,

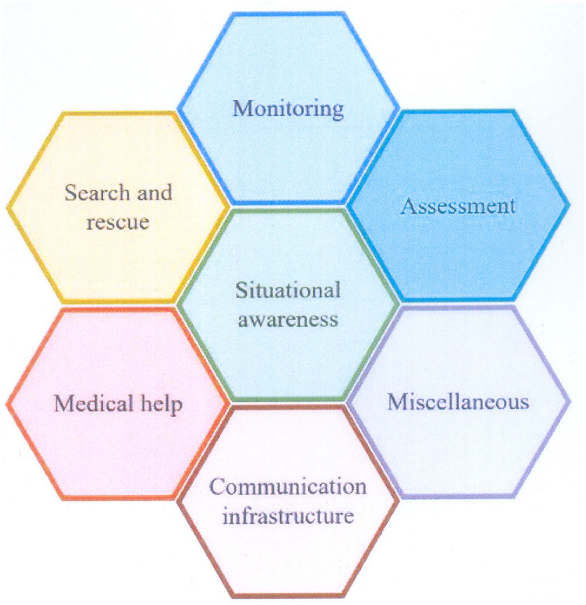

Fig.1 Applications of UAVs in Cataclysm Administration [4]

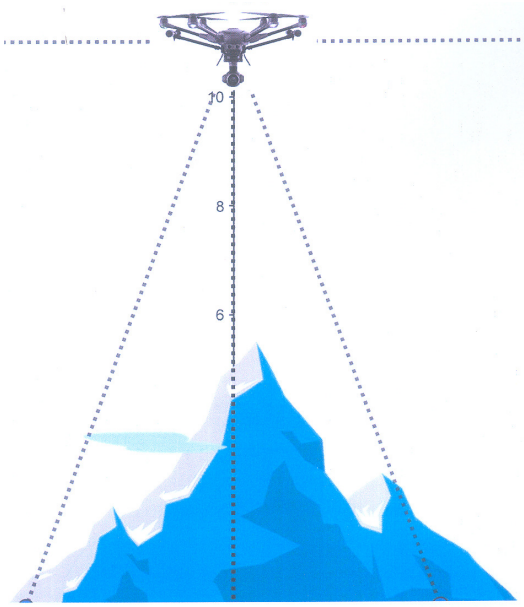

Fig.2 Current Image Acquisition Method by UAVs

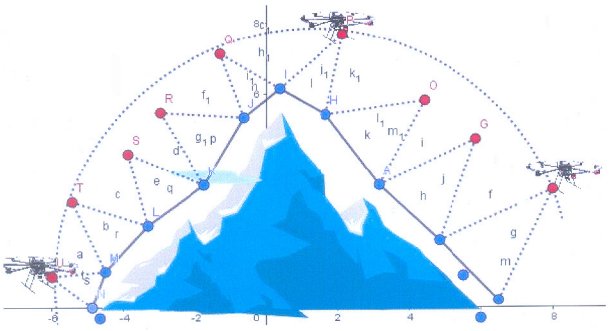

Fig.3 Current Image Acquisition Method by UAVs

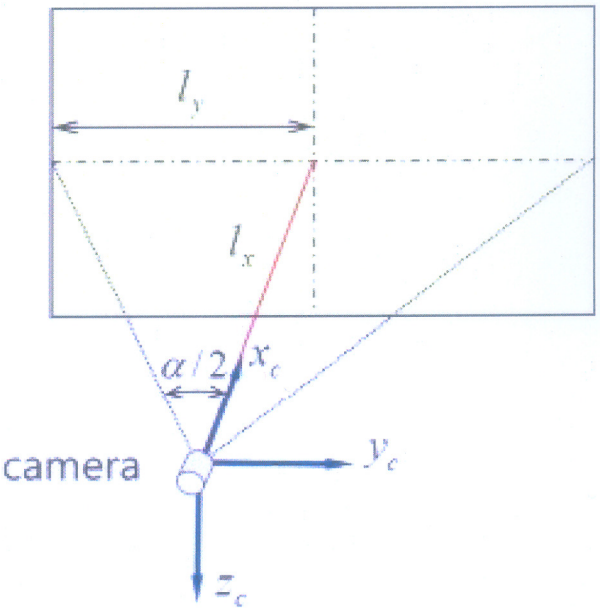

Fig.4 Layout of FOV and Camera Position

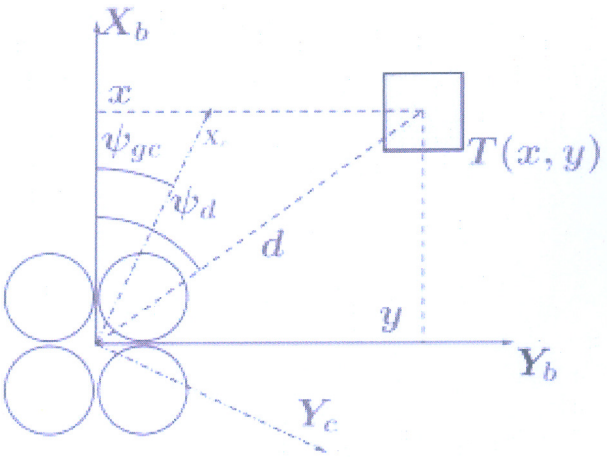

Fig.5 The UAV and the Point of Reference [35]

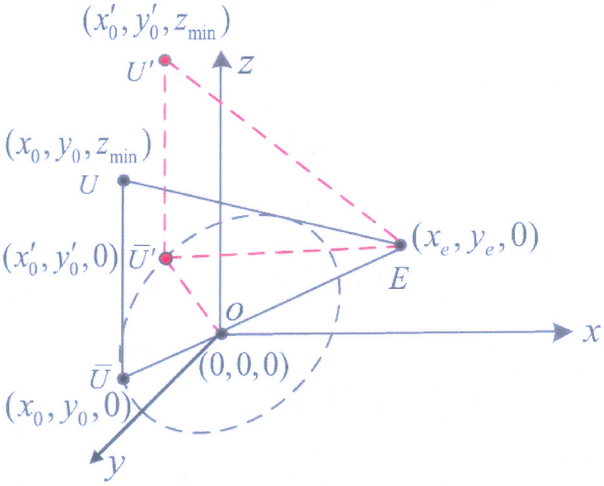

Fig.6 3D Placement of UAV in 3 Axis Coordinate System [15]

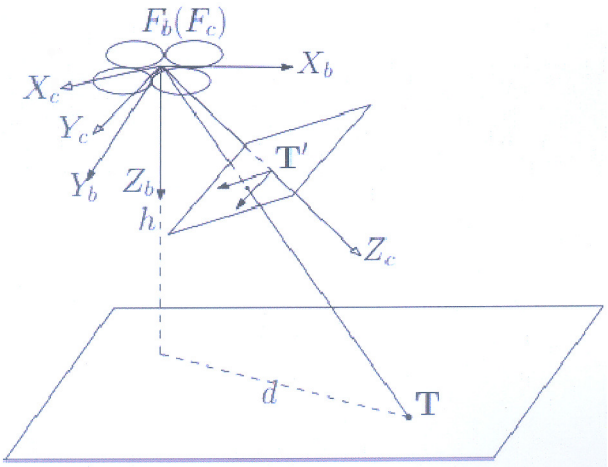

Fig.7 The Relationship Between UAV Camera and the Target Object [35]

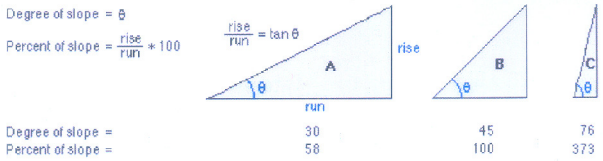

Fig.8 Comparing Values for Slope in Degrees Versus Percent

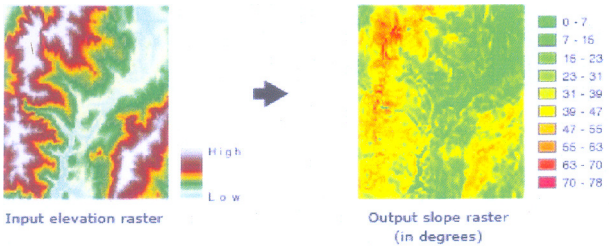

Fig.9 Comparing Values for Slope Mapping

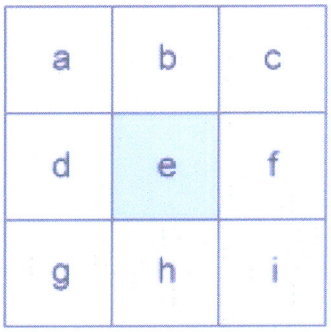

Fig.10 3 x 3 Matrix from DEM

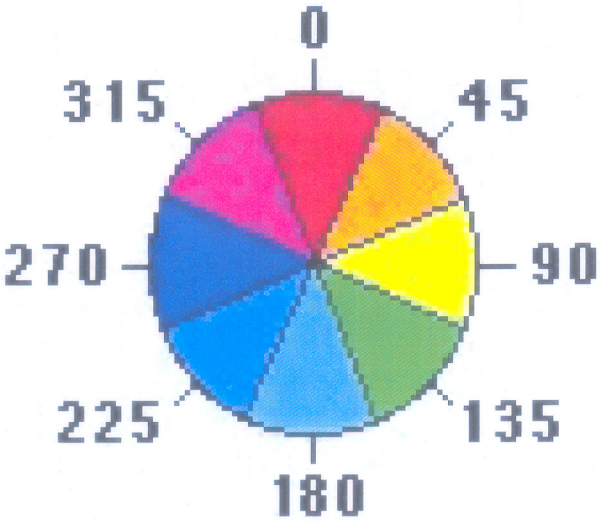

Fig.11 Aspect Directions

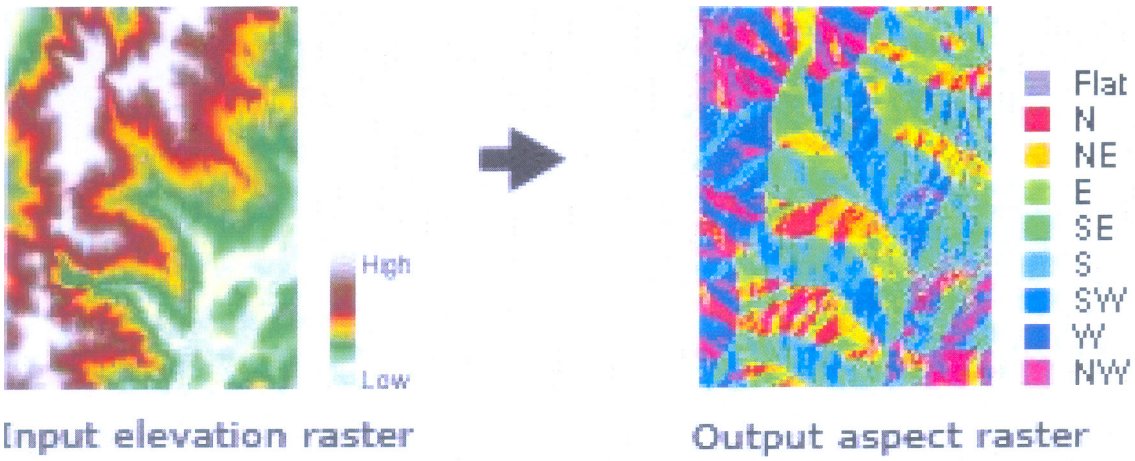

Fig.12 Aspect Directions

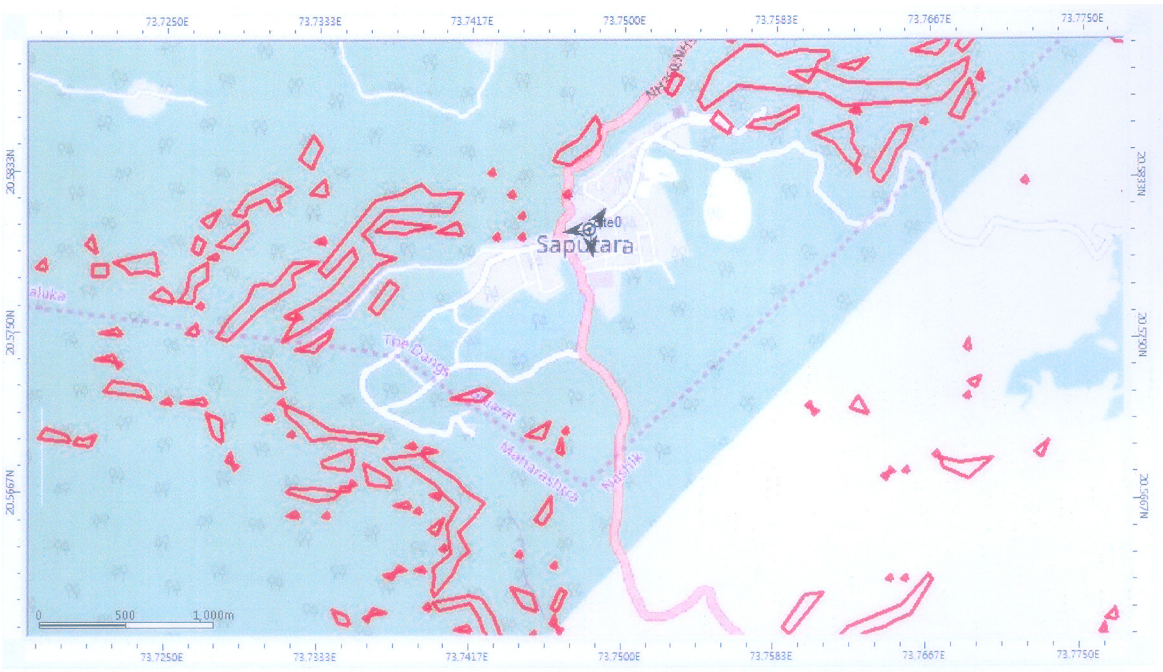

Fig.13 Landslide Risk Zone

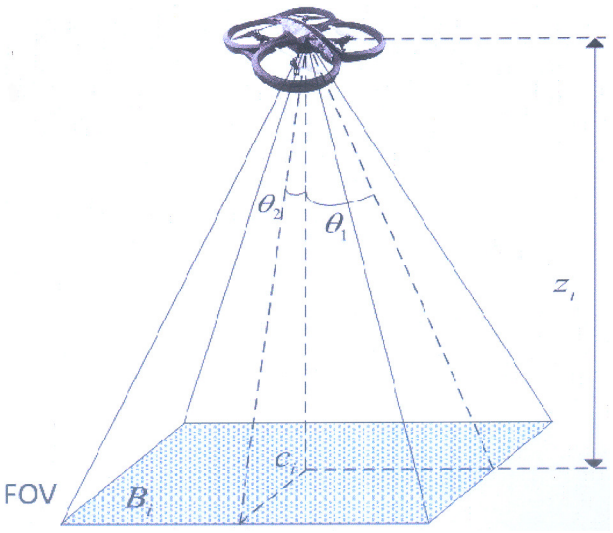

Fig.14 Landslide Risk Zone

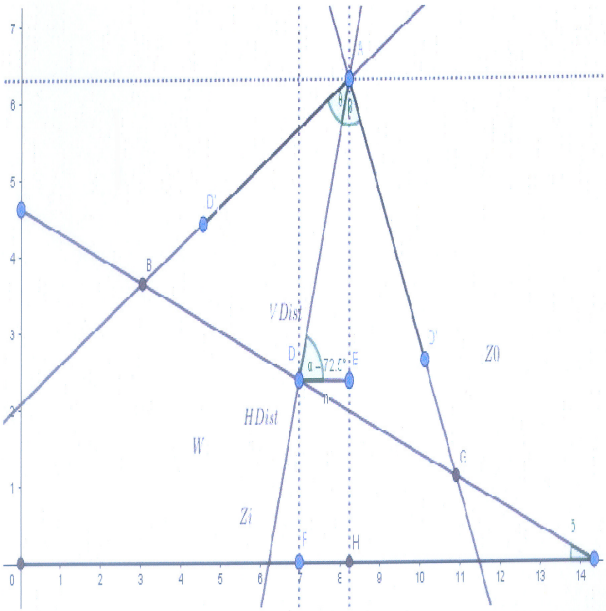

Fig.15 Geometry of Angle of Vision

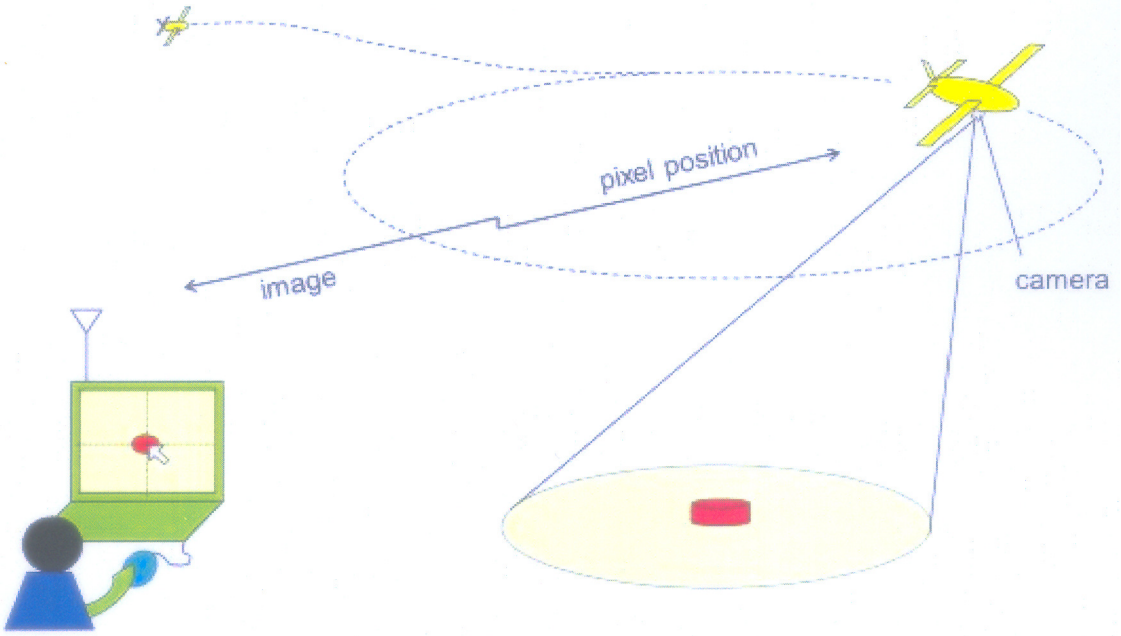

Fig.16 Experimental Setup for Vision-based UAV Position

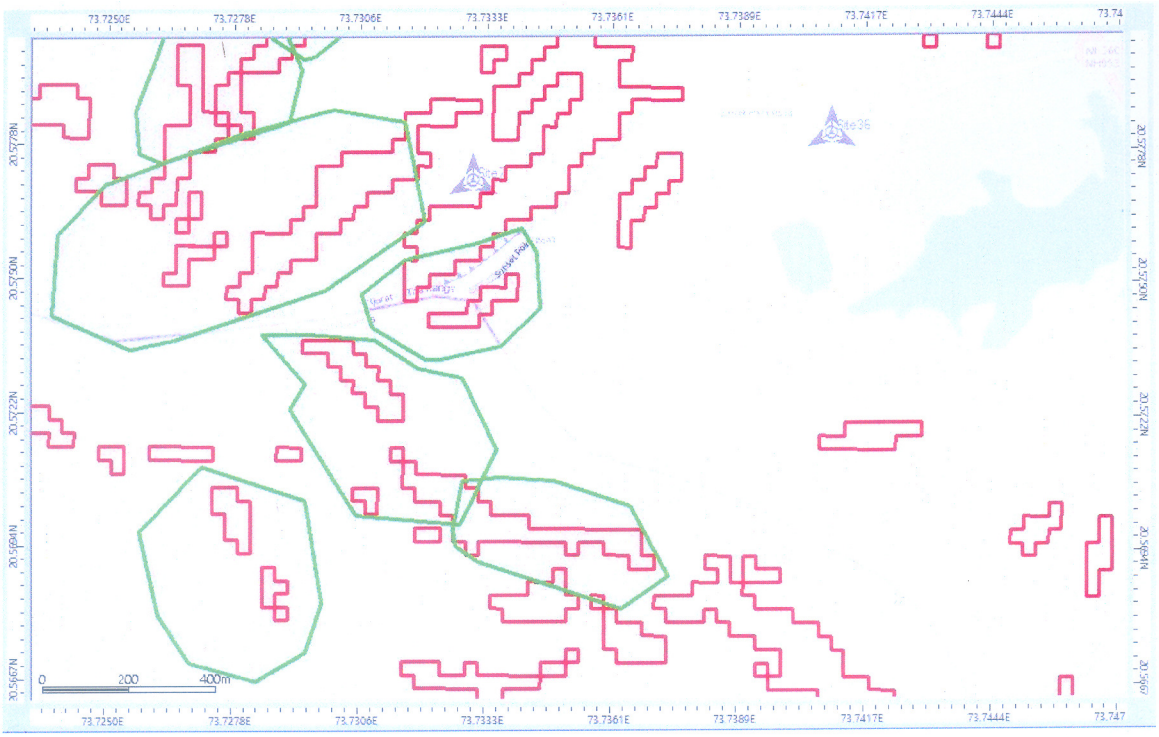

Fig.17 Landslide Risk Zones with Flag Point i.e. Centroid

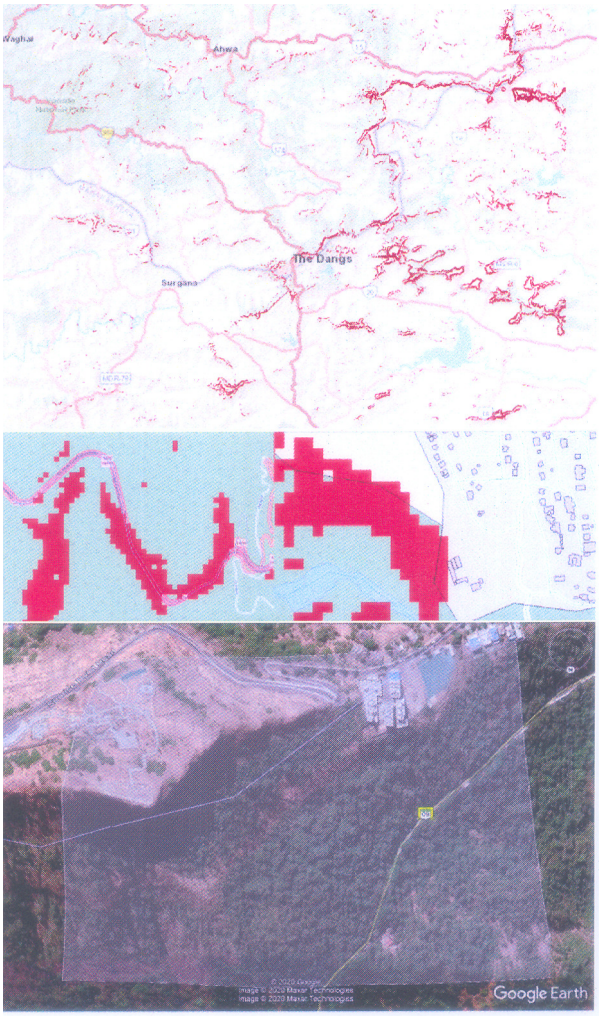

Fig.l8 Landslide Risk Zones Having Slope Greater than 30 Degree

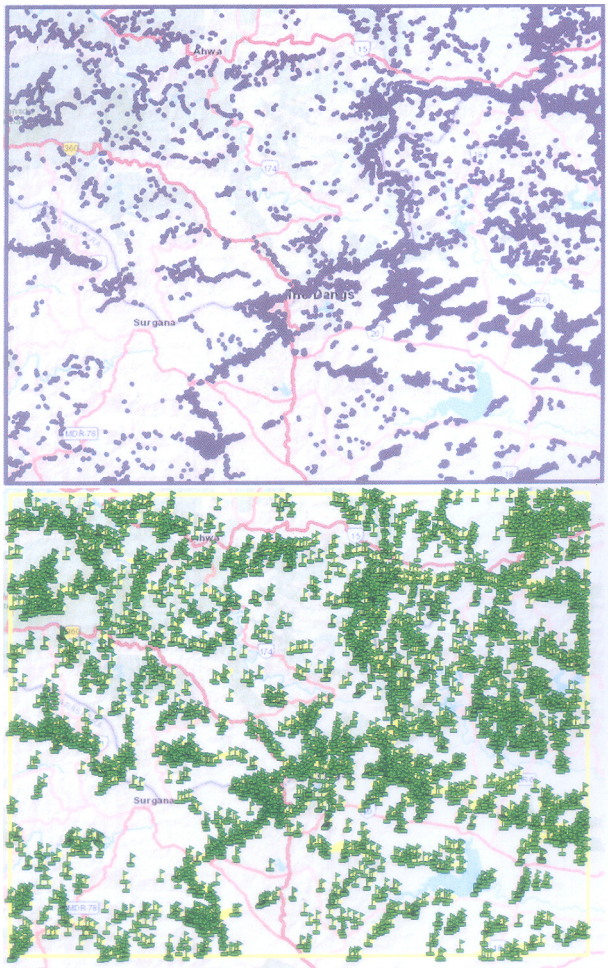

Fig.19 Landslide Risk Zones Having Slope Greater than 30 Degree

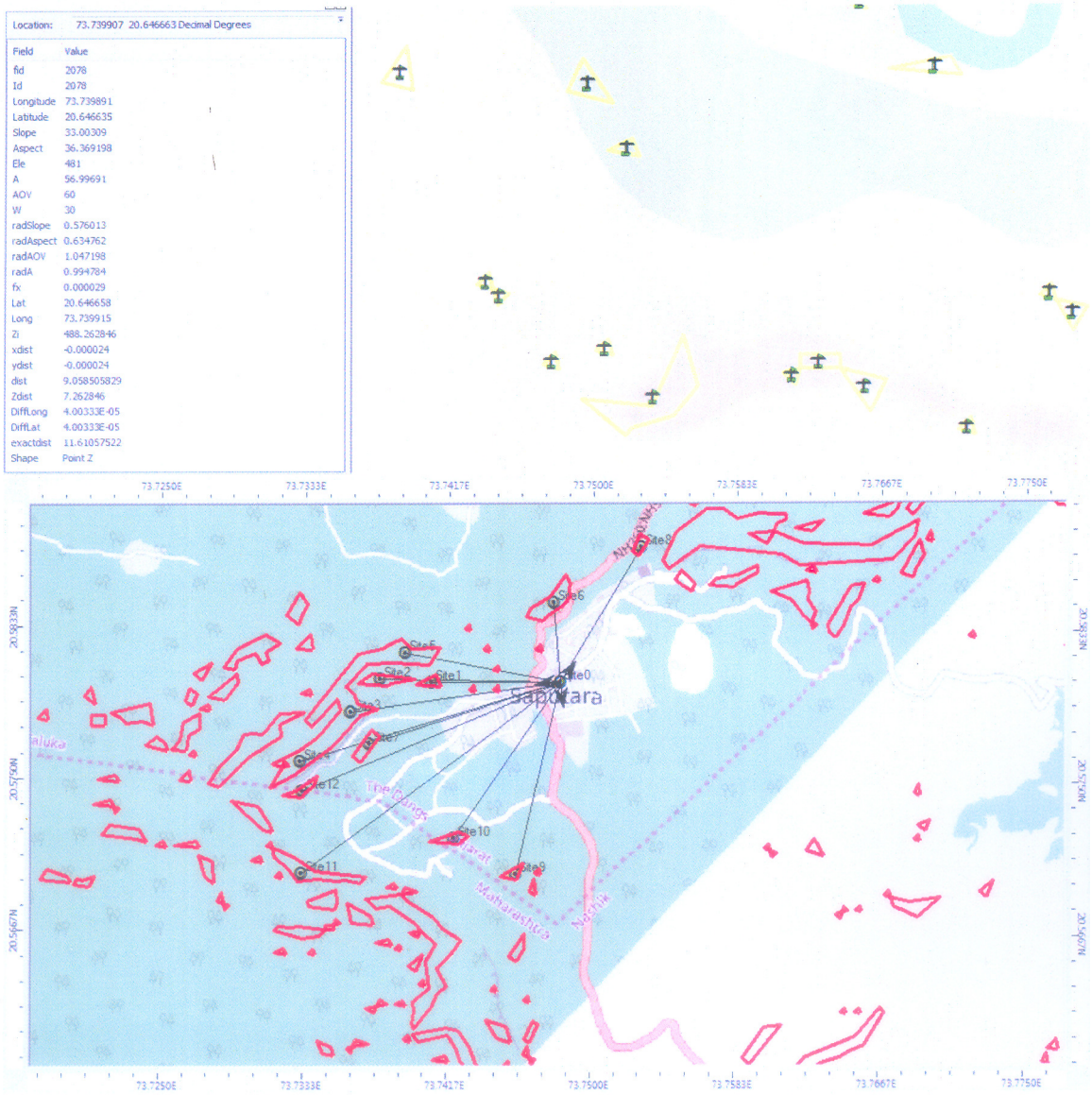

Fig.20 Flag Point of Landslide Susceptibility Index (LSI) and Optimized Geo-positioning Algorithm for UAV

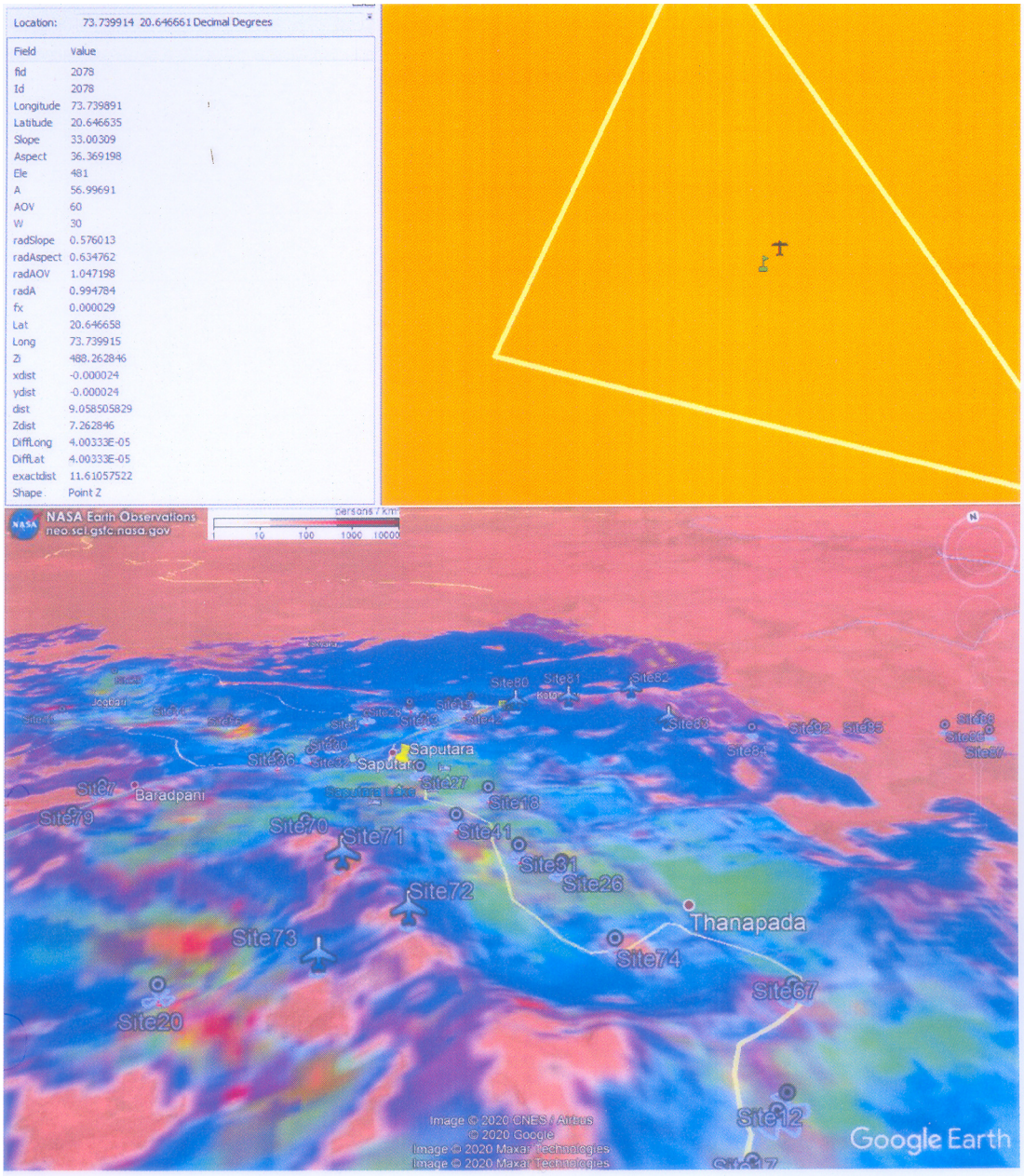

Fig.21 Flag Point Representing the Centroid of Landslide Susceptibility Zone and Flight Point Representing the Actual Optimized Position of Point of View

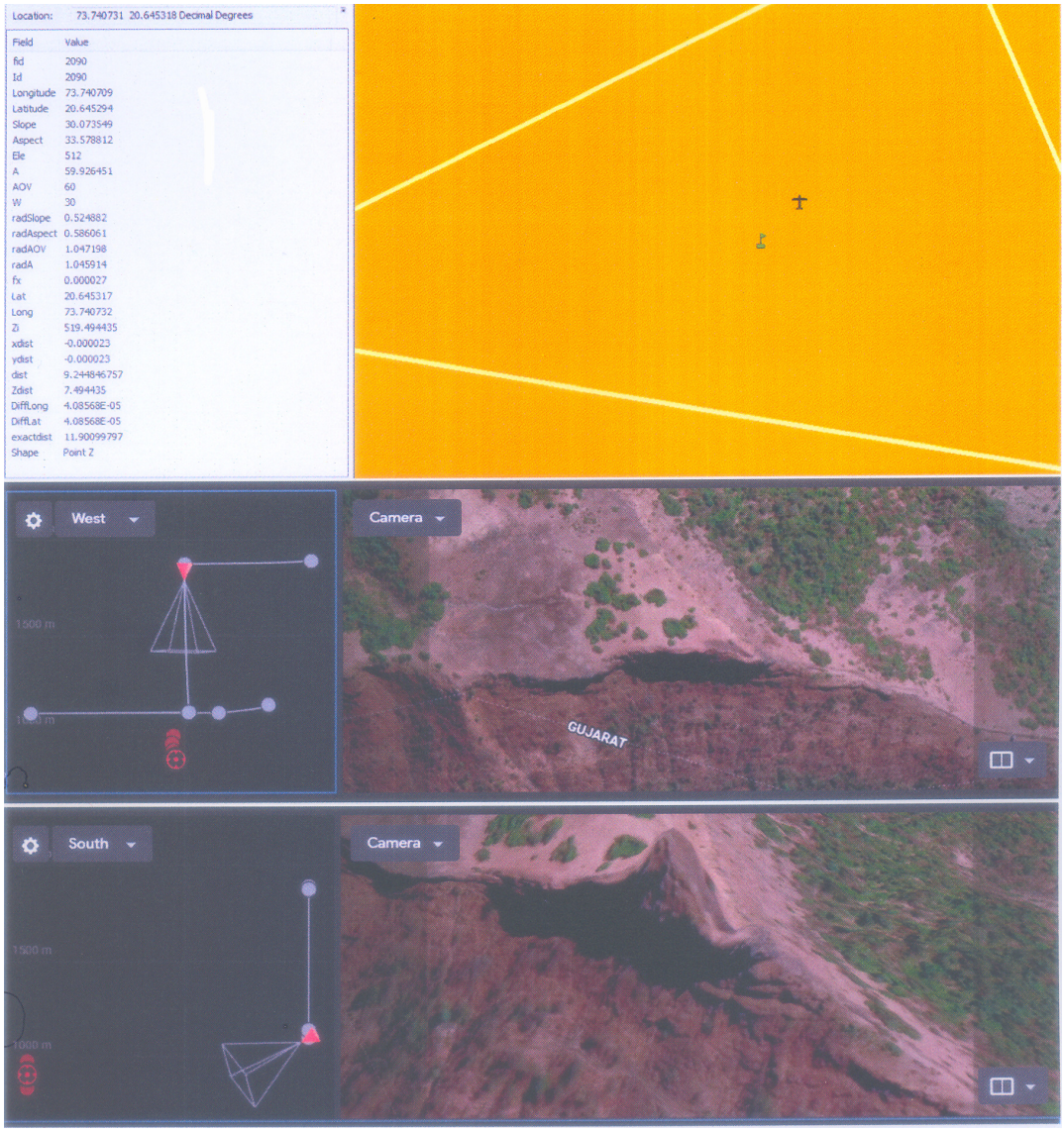

Fig.22 Flag Point Representing the Centroid of Landslide Susceptibility Zone and Flight Point Representing the Actual Optimized Position of Point of View

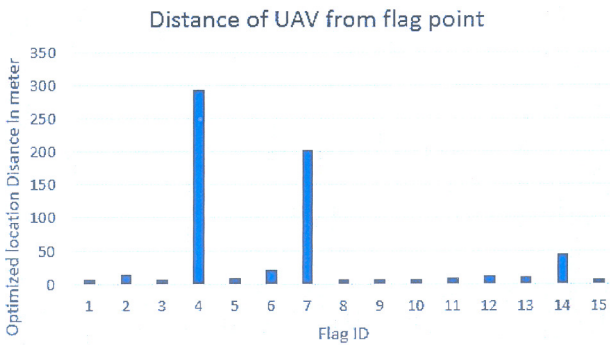

Fig.23 Graph Flag ID Vs Distance in Meters